The Journal of Neuroscience, September 15, 1999, *19*(18):7901–7912

Effects of *roundabout* on Growth Cone Dynamics, Filopodial Length, and Growth Cone Morphology at the Midline and throughout the Neuropile

Michael J. Murray and Paul M. Whitington

Molecular and Cellular Biology, School of Biological Sciences, University of New England, Armidale, NSW 2351, Australia

roundabout (*robo*) encodes an axon guidance receptor that controls midline crossing in the *Drosophila* CNS. In *robo* mutants, axons that normally project ipsilaterally can cross and recross the midline. Growth cones expressing Robo are believed to be repelled from the midline by the interaction of Robo and its ligand Slit, an extracellular protein expressed by the midline glia. To help understand the cellular basis for the midline repulsion mediated by Robo, we used time-lapse observations to compare the growth cone behavior of the ipsilaterally projecting motorneuron RP2 in *robo* and wild-type embyros. In wild-type embryos, filopodia can project across the midline but are quickly retracted. In *robo* mutants, medial filopodia can remain extended for longer periods and can develop into contralateral branches. In many cases RP2 produces both ipsilateral and contralateral branches, both of which can extend into the periphery. The growth cone also exhibits longer filopodia and more extensive branching both at the midline and throughout the neuropile. Cell injections in fixed stage 13 embryos confirmed and quantified these results for both RP2 and the interneuron pCC. The results suggest that Robo both repels growth cones at the midline and inhibits branching throughout the neuropile by promoting filopodial retraction.

Key words: Drosophila melanogaster; roundabout; *growth cone; time-lapse; filopodia; repulsion*

In bilateral animals, structures located at the ventral midline of the developing CNS provide guidance cues that orient the early outgrowth of axons. Repulsive local interactions are thought to play an important role in determining whether axons in close proximity to the midline cross over or project ipsilaterally. In Drosophila, the *roundabout* (*robo*) gene plays a key role in this process (Seeger et al., 1993; Kidd et al., 1998a,b). In *robo* mutants, axons that normally project only ipsilaterally are able to cross and recross the midline. *robo* encodes a receptor with Ig/FNIII extracellular domains and three evolutionary conserved intracellular motifs thought to provide binding targets for other proteins involved in intracellular signaling (Kidd et al., 1998a). *robo* homologs have been found in animals as diverse as mammals (Kidd et al., 1998a) and nematodes (Zallen et al., 1998). Recently it has been shown that the extracellular protein Slit (Rothberg et al., 1988, 1990) is the ligand for Robo (Brose et al., 1999; Kidd et al., 1999) and is also conserved across species (Brose et al., 1999; Li et al., 1999). In *Drosophila*, Slit is expressed by the midline glia and is thought to act as a midline repellent for growth cones expressing Robo. It is not known, however, how Robo affects the behavior of growth cones to bring about this repulsion. Neurons encountering repulsive cues *in vitro* show a range of growth cone behaviors. In some cases, filopodial contact with a repulsive cue can induce changes in adjacent regions of the growth cone, ranging from complete collapse (Kapfhammer and Raper, 1987) to a localized inhibition of lamellipodial protrusion (Fan and Raper, 1995). In other cases, repulsive cues appear to repel only those parts of the growth cone that make physical contact with the cue, leaving the motility of neighboring regions unaffected (Stoeckli et al., 1997).

In this study we have sought to shed light on the cellular basis for axon repulsion mediated by Robo by comparing the growth cone behavior of the motorneuron RP2 in wild-type and *robo* mutant embryos. We have previously described RP2's outgrowth in wild-type embryos as it projects ipsilaterally out of the CNS (Murray et al., 1998). In wild-type embryos, RP2 can extend filopodia across the midline, but these are quickly retracted and do not develop into branches. In *robo* embryos, filopodia can remain extended across the midline for longer periods and can dilate into contralateral branches. In addition we have observed, both at the midline and throughout the neuropile, an increase in the length of filopodia and a more highly branched growth cone. Cell injections of RP2 and of the interneuron pCC in fixed stage 13 embryos confirmed and quantified the results from time-lapse observations. Based on these data, we propose a function for Robo in promoting filopodial retraction to both repel axons at the midline and to inhibit filopodial exploration throughout the neuropile.

MATERIALS AND METHODS

Fly stocks, staging, dissection, culturing, photoconversion, and time-lapse observations. Methods for embryo collection, accurate staging of embryos (for stages 12–14), dissections, cell injections, fixation, photoconversions, and time-lapse observations are as previously described (Murray et al., 1998). Transitional stages (e.g., stage 13/14) denote embryos chosen at the end of one stage and the beginning of the next.

Wild-type embryos were Oregon-R stock.

The *robo* results presented in this article were obtained using the $robo^2$ protein null allele (Seeger et al., 1993; Kidd et al., 1998a), balanced over CyO^{T8LZ} (Kolodziej et al., 1995). $robo^2/robo^2$ mutant embryos were identified by immunostaining for the T8 lacZ insert on the balancer using standard techniques (Patel, 1994). $robo^2/CyO^{T8LZ}$ heterozygotes and

Received April 26, 1999; revised June 22, 1999; accepted June 25, 1999.

This work was supported by an Australian Research Council Large Grant to P.M.W. We thank Corey Goodman and Peter Kolodziej for fly stocks and reagents

Correspondence should be addressed to Dr. Murray at his present address: The Wellcome/CRC Institute, University of Cambridge, Tennis Court Road, Cambridge CB2 1QR, UK.

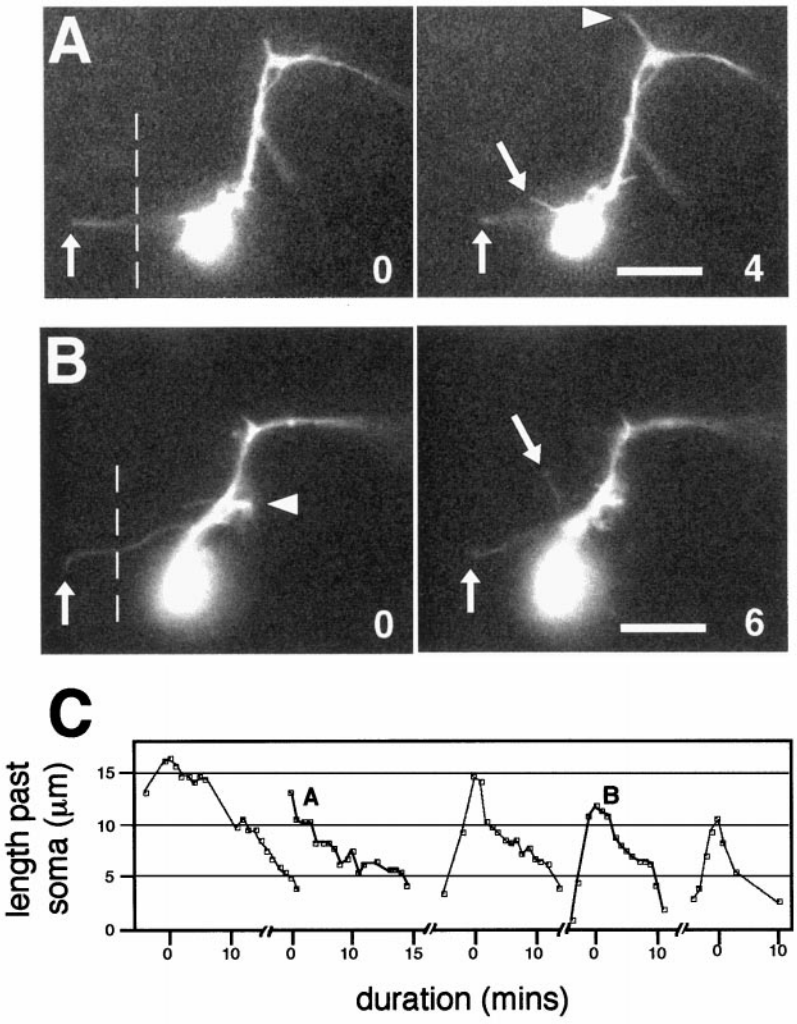

Figure 1. Extension of medial filopodia by RP2 in wild-type embryos. *A*, *B*, Two examples of wild-type time-lapse sequences in which RP2 extends a filopodium medially across the commissures. In this and remaining figures in this article, the midline (indicated by *dotted lines*) is situated to the left of RP2's soma (see image conventions in Materials and Methods). In wild-type sequences the midline was not recorded but is estimated to be ~5 μm from the medial edge of RP2's soma. Filopodia are shown first at their point of maximum extension (*up arrows* at *0* min) and then again shortly afterward, during their retraction (*up arrows*; *A*, *4* min; *B*, *6* min). The extension of new filopodia from adjacent regions of the neuron can continue while the medial filopodium is retracted (*down arrows*; *A*, *4* min; *B*, *6* min). *C*, Time course of extension and retraction of five medial filopodia (taken from the 25 wild-type sequences) that extended ≥10 μm past the medial edge of RP2's soma. Missing data points correspond to frames where the filopodium was out of focus. The second and fourth time courses (*black*) represent the filopodia from Figure 1, *A* and *B*, respectively. Typically a medial filopodium rapidly attains its maximum length, is rapidly partially retracted, and then is fully retracted more gradually. Scale bars, 10 μm.

CyO^{T8LZ}/CyO^{T8LZ} homozygotes were distinguished by staining intensity.

Cell injections of RP2 and pCC were also performed in fixed stage 13–14 embryos, homozygous for *robo*^{1}, another protein null allele (Kidd et al., 1998a). The conclusions based on these data were the same as those for *robo*^{2}; i.e., that RP2 can project contralaterally and ipsilaterally and can bifurcate into both contralateral and ipsilateral branches; that pCC can also bifurcate into ipsilateral and contralateral branches; and that both RP2 and pCC growth cones are more highly branched and tend to have longer filopodia than wild-type. The length of filopodia was quantified for RP2 (n = 30 cells) in *robo*^{1}/*robo*^{1} embryos and had a mean value and distribution not significantly different from *robo*^{2} results.

Filopodial analysis in time-lapse sequences. The time-lapse results presented in this article are based on 23 *robo* sequences and 25 wild-type sequences, 22 of which have been presented previously (Murray et al., 1998). The analysis of long (≥9 μm) filopodia was restricted to time-lapse sequences with sufficient image clarity to allow filopodia to be resolved (n = 17 for wild-type and n = 22 for *robo*). Because time-lapse sequences are restricted to a single focal plane, it is possible that filopodia oriented in a dorsoventral direction have escaped detection. In addition, filopodia that were measured were not always fully in focus at the time when they reached their maximum length (see Fig. 3, *arrowhead* at *13* min). In these cases an estimate was made of the extent of the filopodium based on previous or later frames that more clearly showed the region from which the filopodium originated (see Fig. 3, *arrowhead* at *9* min).

Filopodial analysis in stage 13 fixed embryos. Embryos were chosen at midstage 13, dissected in saline, and immediately fixed. Cells were injected with DiI, and a z-stack of images were collected at 0.5 μm intervals. Z-motor control was as described previously (Murray et al., 1998). Filopodia were identified as that population of processes of minimum caliber (~0.25–0.35 μm apparent width in fluorescent images) with uniform thickness and uniform labeling to their tip. Filopodia were measured from their tip inward, up to the point at which the thickness increased or a branch point was reached. Measurements were performed with Object-Image, a variant of the NIH-Image program (available at http://rsb.info.nih.gov/nih-image/), which permits measurement of objects that extend across multiple image planes.

Image conventions. All images in this article are dorsal views of the exposed CNS in a flat dissection with anterior upward. Cell injections of RP2 and pCC are from both sides of the midline, but for consistency they have been horizontally flipped in Figures 2*A–E* and 4*B* so that the midline is always to the left of the soma.

RESULTS

Time-lapse observations of RP2 in wild-type embryos

We have previously characterized the wild-type behavior of RP2's growth cone as it navigates out of the CNS (Murray et al., 1998). RP2's axon initially extends a short distance anterolaterally, then turns more anteriorly along the longitudinal connectives and finally turns laterally along the intersegmental nerve (ISN) and into the periphery. Although RP2 projects ipsilaterally, filopodia do explore the contralateral direction across the commissures (Fig. 1*A*, *up arrow*, *0* min; *B*, *up arrow*, *0* min). The position of the midline was not documented during wild-type time-lapse sequences but averages ~5 μm from the medial edge of RP2's soma in filleted embryos for the stages used. Filopodia extending to or past this point were not uncommon, occurring on 10 occa-

sions in the 25 wild-type sequences. In five of these cases the filopodium extended >5 μm past the estimated position of the midline before being retracted. The time course of extension and retraction of these medial filopodia is shown in Figure 1*C*. Typically a medial filopodium rapidly attains its maximum length, is rapidly partially retracted, and then is fully retracted more gradually. The retraction of medial filopodia does not preclude the extension of new filopodia in adjacent regions of the neuron (Fig. 1*A*, *down arrow*, *4* min; 1*B*, *down arrow*, *6* min).

Filopodia in nonpathway directions can develop into transient branches, but these are resorbed as the main branch matures. These arise most commonly at the two points where RP2's axon turns more anteriorly ($n = 5$ of 25 sequences) (Fig. 1*B*, *arrowhead*, *0* min) and where it turns laterally ($n = 16$ of 25 sequences) (Fig. 1*A*, *arrowhead*, *4* min). Filopodia extending medially across the commissures did not form branches, although in one case there was a slight thickening at the base of the filopodium toward the end of its retraction.

Axonal trajectory of RP2 in *roundabout* embryos

Given RP2's proximity to the midline and the fact that it can extend filopodia across the commissures in wild-type embryos, we wondered whether RP2's axon might cross the midline in *robo* mutant embryos. To determine the axonal trajectory of RP2 in *robo* embryos, we iontophoretically labeled RP2's soma with DiI in fixed embryos at stages ranging from midstage 12 to stage 16.

We find that in many cases RP2 does produce a contralateral branch, which after crossing the midline follows the same pathway as the normal ipsilateral branch: anteriorly up to the ISN and then laterally out of the CNS along the ISN (Fig. 2*A*). The formation of a contralateral branch does not preclude the formation of the normal ipsilateral branch with RP2 displaying a spectrum of phenotypes ranging from completely contralateral (Fig. 2*A*), to bifurcating into contralateral and ipsilateral branches (Fig. 2*B*), to completely ipsilateral (Fig. 2*C*). The length of contralateral branches does not appear to be correlated with the developmental stage of the embryo.

As shown in Table 1, the analysis concentrated on stages 13–14. At later stages soma positions in the CNS become progressively less predictable, and injection of RP2 is difficult. The few results obtained at stages 15–16 show that RP2's contralateral branch can continue into the periphery. We also find that when RP2 bifurcates into two axons, both can project into the periphery, indicating that the ectopic branches can be as stable as ipsilateral branches (Fig. 2*D*), although it is not known whether contralateral branches eventually synapse with their appropriate target muscle. In one stage 16 embryo, RP2's axon projected contralaterally but then turned posteriorly rather than anteriorly, exited the CNS in the next posterior ISN, extended under the ventral muscles, and was exploring the dorsal muscle field (Fig. 2*E*). Thus RP2's axon is not restricted to the normal anterior pathway (ipsilateral or contralateral) but does appear to selectively exit via the ISN despite the proximity of the segmental nerve. The relative frequencies of different axon morphologies from these injections are summarized in Table 1. Aberrant axonal trajectories accounted for approximately one-half the total.

In addition to aberrant axonal trajectories, *robo* cells exhibited differences in growth cone morphology from wild-type cells. Figure 2*F* shows a typical wild-type growth cone morphology at midstage 13 consisting of a single dominant branch projecting along the normal pathway, and 13 filopodia ranging in length from 1 to 4 μm. In contrast, *robo* growth cones tend to have longer filopodia (Figs. 2*G*,*H*, *arrowheads*) and be more highly branched (Fig. 2*B*,*C*,*G*,*H*). These branches are often unusually long and thin (Fig. 2*B*, *arrow*) in comparison with wild-type axons at a similar stage (Fig. 2*F*).

Time-lapse observations of RP2 in *roundabout* embryos

To observe RP2's growth cone behavior in *robo* mutants, and in particular to watch the formation of RP2's contralateral branch, we collected 23 time-lapse sequences in *robo* mutant embryos. Twenty-two sequences were begun at early stage 13 and one at midstage 12.

The time-lapse sequences displayed a range of axonal trajectories similar to those seen in cells injected in fixed embryos. Of the 23 sequences, 16 neurons extended a normal ipsilateral branch that projected anteriorly to the ISN and then laterally along the ISN (Fig. 3), one extended a normal ipsilateral branch but then subsequently also developed a contralateral branch that projected out the contralateral ISN, two projected contralaterally and extended out the contralateral ISN (Fig. 4*A*), two projected contralaterally but had not reached the ISN at the end of recording (Fig. 4*B*), one produced an ipsilateral posterior branch (Fig. 4*C*), and one produced both an ipsilateral anterior branch and an ipsilateral posterior branch that itself bifurcated.

In a number of cases transient branches formed but were retracted as another was formed. For example in Figure 4*B1*, an initial ipsilateral branch (*arrow* at *0* min) is resorbed as a contralateral branch forms (*arrow* at *105* min). In Figure 4*C*, an anterior ipsilateral branch (*right arrow* at *28* min) is retracted as a posterior branch forms (*arrowhead* at *131* min).

Of the five time-lapse sequences in which a contralateral branch formed, three were observed as they occurred (one had already occurred and one occurred out of the plane of focus). In these three cases the formation of the contralateral branch appeared to follow a normal wild-type axon-advancement sequence, in which a filopodium undergoes dilation (Fig. 4*A*, 39–66 min; 4*B2*). New filopodia then extended from this more advanced position.

In addition to these cases in which the contralateral branch formed and persisted until the end of recording, there were 19 cases in which filopodia were able to cross the midline for extended periods (up to 56 min), in some cases thickening into transient branches, before being resorbed. For example, in Figure 4*C*, a filopodium extends across the midline (*down arrows*, *28–34* min) and subsequently thickens (*down arrow* at *38* min). The resultant medial branch remains extended and continues to extend filopodia (*down arrow* at *43* min) before being finally resorbed. In Figure 5*A*,*B*, a medial filopodium extends to a maximum distance of ~10 μm past the midline before being finally retracted after 30 min. To quantify changes in the persistence of medial filopodia in wild-type and *robo* sequences, we measured the period in which a filopodium (or subsequent branch) remained extended past the midline for the two genotypes. RP2's soma position is more variable in *robo* embryos and in some cases is displaced toward the midline. The distance from RP2's soma to the midline averaged 3 μm in *robo* time-lapse sequences. To allow for the possibility that any increased persistence in *robo* embryos was caused by this difference in soma-midline distance, wild-type results were calculated assuming soma-midline distances of both 5 and 3 μm. The results (Fig. 5*D*) show that in both cases medial filopodia in *robo* embryos tended

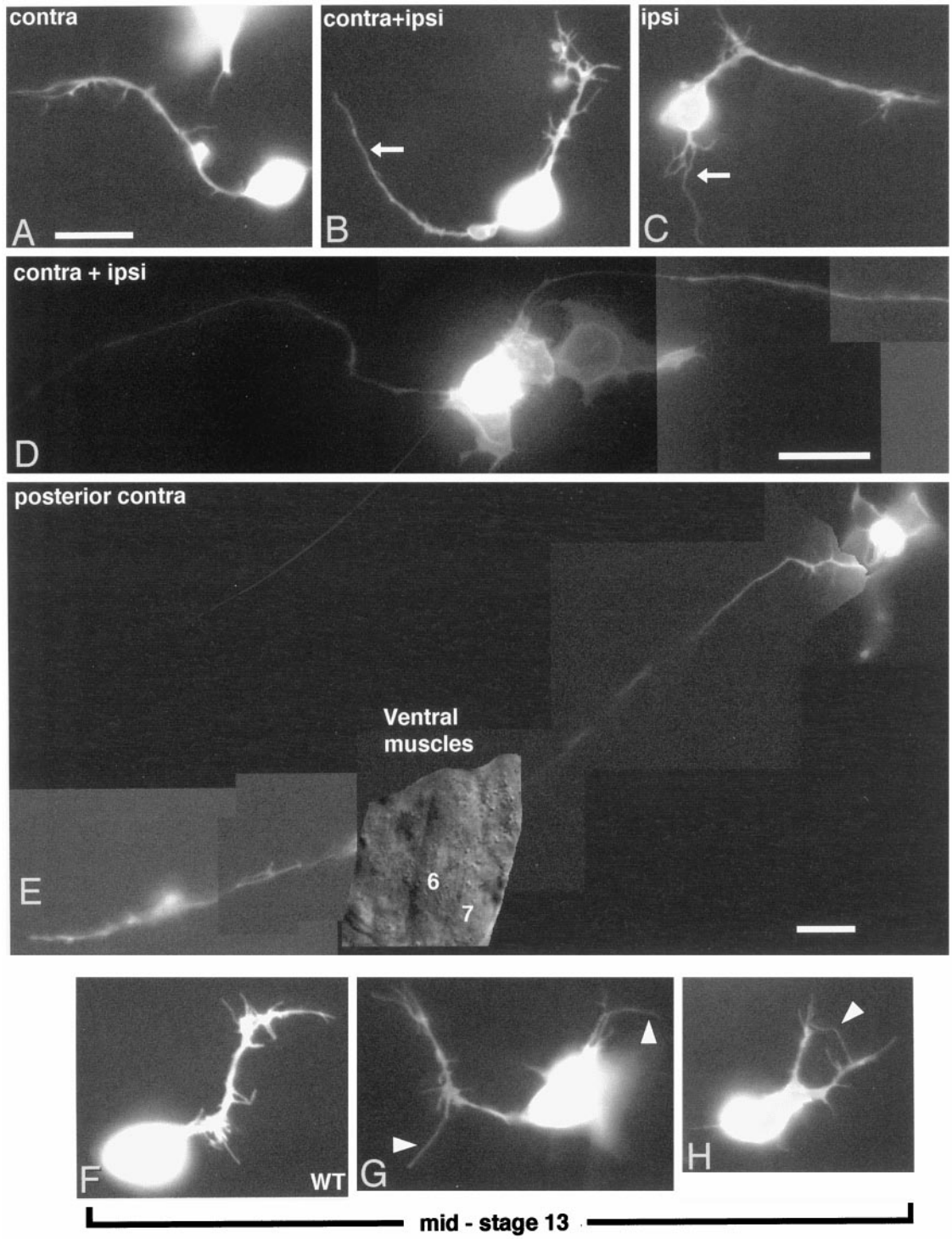

Figure 2. Axonal trajectories and growth cone morphologies of RP2 in *robo* mutant *(A–E, G, H)* and wild-type (*F*) embryos. *A*, Stage 13/14 *robo* embryo. RP2 has developed a contralateral branch that, after crossing the midline, follows the usual pathway anteriorly along the longitudinal connectives and then laterally along the ISN. *B*, Stage 14 *robo* embryo. RP2 has developed both a normal ipsilateral branch and a long thin contralateral branch (*arrow*). *C*, Stage 14/15 *robo* embryo. RP2 has extended a normal ipsilateral branch but has also developed a branch in the ipsilateral posterior direction (*arrow*). *D*, Stage 15 *robo* embryo. RP2 has bifurcated into ipsilateral and contralateral branches, both of which have exited the CNS. *E*, Stage 16 *robo* embryo. RP2 has projected contralaterally, but then turned posteriorly, has exited the CNS in the next posterior ISN, has passed under the ventral muscle field, and is exploring the dorsal muscle region. *F*, Midstage 13 wild-type embryo. RP2 displays a typical growth cone morphology for this developmental stage consisting of a single dominant axonal branch with 13 filopodia ranging in length from ~1 to 4 μm. *G*, Midstage 13 *robo* embryo. RP2 has developed a contralateral branch that has crossed the midline and migrated anteriorly to the contralateral ISN. Filopodia are longer than usual, ranging from ~1 to 8 μm, and are exploring the normal ipsilateral direction and the contralateral posterior direction (*arrowheads*). *H*, Midstage 13 *robo* embryo. RP2 has developed two ipsilateral branches and has an unusually long (9 μm) filopodium (*arrowhead*). Scale bars (shown in *A* for *B*, *C*, *F–H*): 10 μm.

Table 1. Axonal trajectories of RP2 in *robo* mutants

	Developmental stage			
RP2's axonal trajectory	12/13 (6)	13 (15)	13/14 (16)	≥14 (9)
Contralateral	1	1	0	5[a]
Mainly contralateral	1	1	1	1
Contralateral and ipsilateral	4	8	7	5
Mainly ipsilateral	4	6	6	2
Ipsilateral	8	14	28	16
Total cells injected	18	30	42	29
% aberrant	56%	53%	33%	45%

RP2 was injected with DiI in embryos fixed at successive developmental stages. Column headings give the embryonic stage. Numbers in parentheses give the number of embryos injected.

[a] This includes the cell shown in Figure 2*E* that was contralateral but projected posteriorly.

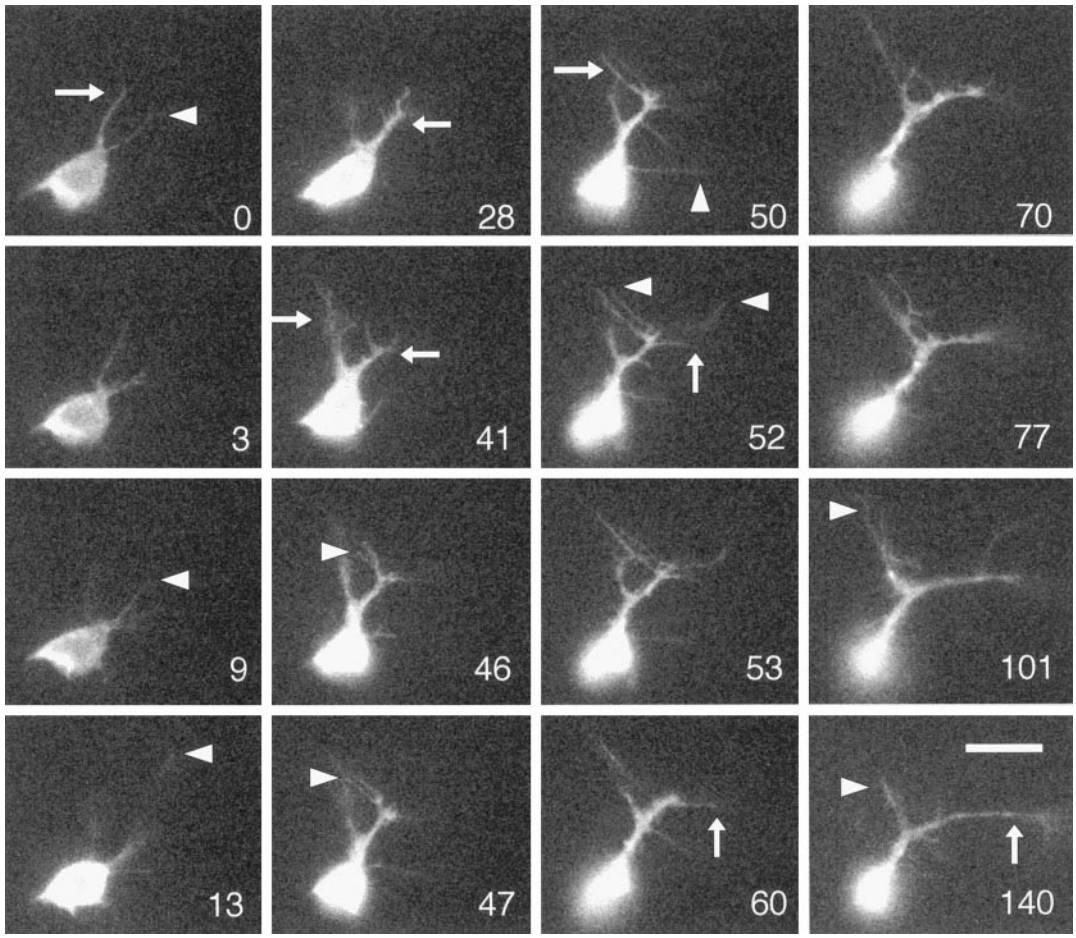

Figure 3. *robo* sequence in which RP2 extends an ipsilateral axon. At *0* min RP2 has developed an ipsilateral branch (*arrow*) and extends a filopodium along a more lateral ipsilateral pathway (*arrowhead*). The more lateral branch continues to develop with the extension of a long filopodium (*arrowheads*, *9–13* min) that subsequently thickens (*arrow* at *28* min), resulting in two ipsilateral branches (*arrows* at *41* min). RP2 begins to extend numerous long filopodia (*arrowheads* at *46–47*, *50*, *52* min), some of which thicken (*right arrow*, *50* min), resulting in a highly branched morphology (*53* min). During this period, RP2 extends a filopodium in a lateral direction (*up arrow* at *52* min) that thickens (*up arrow*, *60* min), redirecting the axon laterally (*up arrow, 140* min). The original ipsilateral branch continues to extend new filopodia (*arrowhead* at *101* min) and persists to the end of recording (*arrowhead* at *140* min). Scale bar, 10 μm.

to remain extended across the midline for longer periods than in wild-type sequences.

There was also a difference in the behavior of medial filopodia. In Figure 5*C* the time course of extension and retraction of the filopodium in Figure 5*B* is contrasted with the wild-type filopodium in Figure 1*B*. Where the wild-type filopodium is quickly retracted after reaching its maximum length, the *robo* filopodium repeatedly extends and retracts as it explores the contralateral side before being fully retracted.

Another feature of time-lapse sequences was a tendency for the growth cone to produce an excess of long (≥9 μm) filopodia. In normal wild-type sequences, long filopodia do occasionally occur

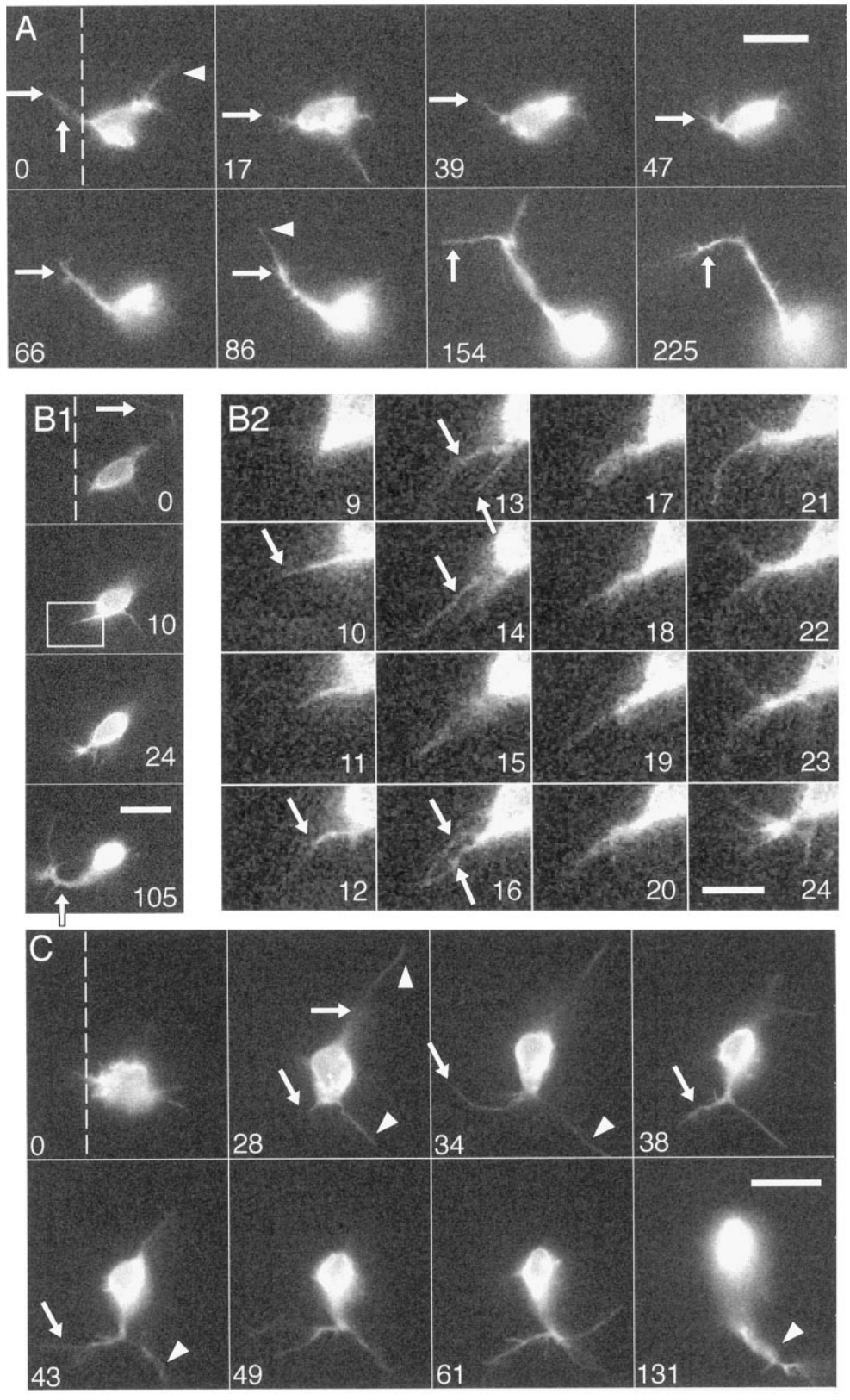

Figure 4. *robo* sequences in which RP2 extends axons in aberrant directions. *Dotted lines* show position of the midline. *A*, RP2 develops a contralateral axon. At *0* min, RP2 has extended a filopodium in the ipsilateral direction (*arrowhead*) and two filopodia (*right arrow* and *up arrow*) in a contralateral direction. At *17* min the ipsilateral filopodium and more posterior of the two contralateral filopodia have been retracted. The more anterior contralateral filopodium thickens but is then retracted (data not shown). At *39* min a new filopodium extends contralaterally (*right arrow*, *39* min) and subsequently thickens into a contralateral branch (*right arrows*, *47–86* min). Having crossed the midline, the axon migrates anteriorly along the longitudinal connectives (*arrowhead* at *86* min) and extends a lateral filopodium at the ISN (*arrow* at *154* min), which subsequently thickens, redirecting the axon along the contralateral ISN (*up arrow* at *225* min). *B,* RP2 develops a contralateral branch. *B1*, At *0* min RP2 has a process in the ipsilateral direction (*arrow*) that is retracted as the contralateral branch (*arrow* at *105* min) develops. *B2*, Detail of branch formation from 9 to 24 min. From 9 to 10 min, a filopodium extends in a contralateral direction (*arrow* at *10* min) and thickens (*arrow* at *12* min). In subsequent frames a second filopodium extends (*up arrow* at *13* min) and also thickens (*up arrow* at *16* min), resulting in two contralateral processes (*arrows* at *16* min). These appear to merge as the contralateral branch matures and new filopodia extend from its tip (*24* min). *C*, RP2 develops an ipsilateral posterior branch. At *0* min RP2 is still undergoing axonogenesis and is extending filopodia in all directions. By *28* min RP2 has developed an ipsilateral branch (out of focus; *right arrow* at *28* min) with a filopodium extending from the tip of this branch along the ipsilateral pathway (*up arrowhead* at *28* min). From the posterior side of the soma, another ipsilateral filopodium extends and develops into an ipsilateral posterior branch (*down arrowheads* at *28*, *34*, *43*, and *131* min). At 28 min another filopodium emerges from the posterior side of the soma (*down arrow*), extends across the midline (*down arrow* at *34* min), and begins to thicken (*down arrow* at *38* min). New filopodia continue to explore the contralateral direction (*down arrow* at *43* min), but the contralateral branch is eventually resorbed as the ipsilateral posterior branch matures (*arrowhead* at *131* min). Scale bars: *A*, *B1*, *C*, 10 μm; *B2*, 5 μm.

in nonpathway directions (e.g., the medial filopodia shown in Fig. 1), but for the most part they are restricted to the lateral turn at the ISN. In *robo* sequences there are numerous cases in which long filopodia are extended in other directions (Fig. 3, *arrowheads* at *13*, *50*, *52* min; Fig. 4*C*, *arrowheads* at *28*, *34* min; Fig. 5*B*, *18* min). These filopodia often thicken, producing long thin branches that are subsequently retracted (Fig. 3, *right arrow* at *50* min; Fig. 4*C*, *arrow* at *38* min; Fig. 5*B*, *28* min). The tendency for filopodia to thicken often resulted in a more highly branched morphology (Fig. 3, *53* min; Fig. 4*C*, *61* min). Maximum observed rates of

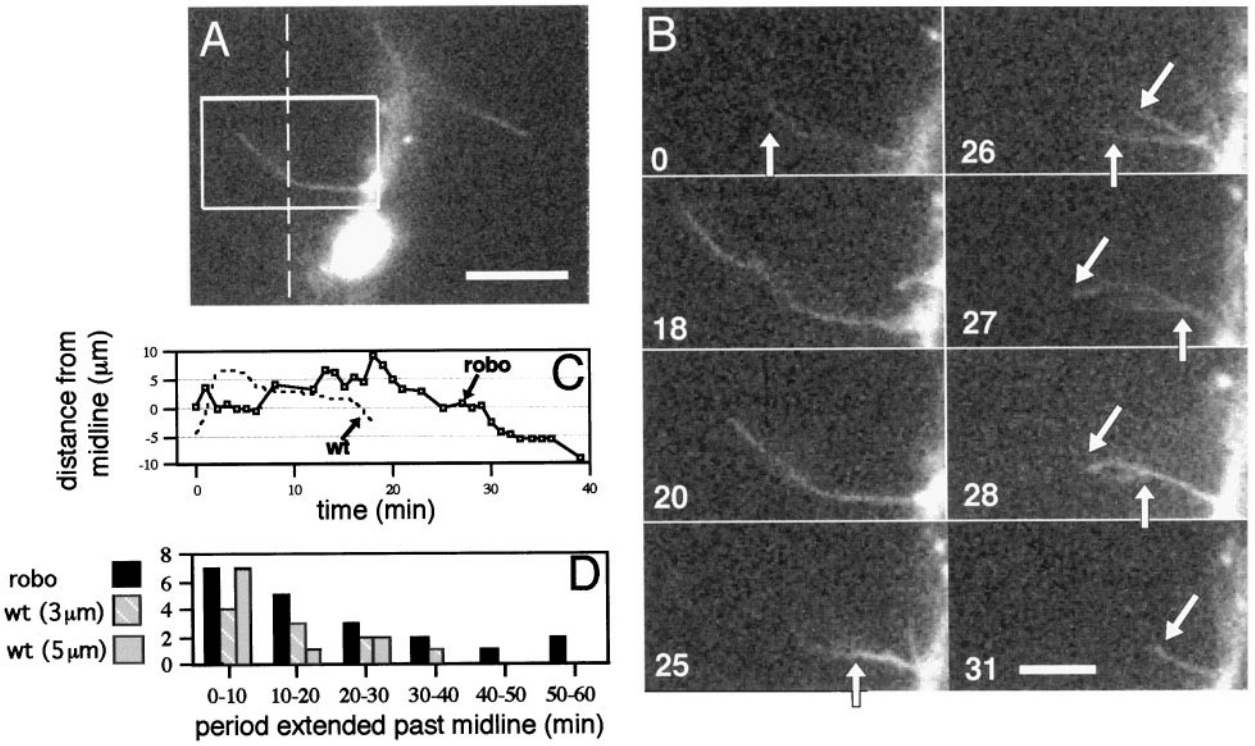

Figure 5. *robo* sequence showing the time course of a medial filopodium. *A*, RP2 has extended a normal ipsilateral branch that is turning laterally along the ISN. *Dotted line* shows position of the midline. *B*, Detail of *A* showing extension of medial filopodium over a period of 30 min. Filopodium is first detected at a length of ~9 μm (*up arrow* at *0* min) and extends to a maximum length of 18 μm (*18* min). At *25* min the filopodium thickens (*up arrow*), and a new filopodium extends from this thickened region (*down arrow* at *26–27* min). The original filopodium is retracted, and its base appears to be translocated forward along the new filopodium (*up arrow* at *27–28* min). The combined process is then retracted and disappears at 39 min (data not shown). *C*, Time course of extension of filopodium with time course of wild-type filopodium from Figure 1*B* overlaid. Where the wild-type filopodium is quickly retracted after reaching its maximum length, the *robo* filopodium repeatedly extends and retracts as it explores the contralateral side before being fully retracted. *D*, Histogram of the period spent extended across the midline for filopodia and any subsequent transient branch that formed (Fig. 4*C*, *down arrow* at *38* min) in *robo* and wild-type sequences. Wild-type values were calculated using both 5 and 3 μm as the estimated position of the midline from the medial edge of RP2's soma (see Results). In both cases the *robo* medial filopodia tended to remain extended past the midline for longer periods of time. Scale bars: *A*, 10 μm; *B*, 5 μm.

filopodial extension and retraction were ~5 μm/min as for wild-type sequences.

In an attempt to quantify the tendency for formation of longer filopodia, we measured filopodia of ~9 μm or greater in wild-type and *robo* sequences (difficulties in this process attributable to image clarity and the restriction of a single focal plane are discussed in Materials and Methods). Measurements were pooled for each genotype, and a histogram of filopodial length was calculated and normalized to account for the total duration of the sequences (Fig. 6*A*). In addition, a cumulative histogram, showing the number of filopodia greater than a given length, was calculated (Fig. 6*B*). These data show that in *robo* time-lapse sequences the frequency of long filopodia is higher than in wild-type sequences.

Filopodial length distributions of RP2 in midstage 13 embryos

To more accurately quantify the length of filopodia, we performed detailed measurements of cells injected in embryos fixed at an accurately determined developmental stage. RP2 was injected with DiI in midstage 13 embryos, and a z-stack of images was collected at 0.5 μm intervals. Measurements were obtained for *robo*/*robo* ($n = 22$), *robo*/CyO ($n = 32$), CyO/CyO ($n = 17$), and wild-type ($n = 31$) embryos (see Fig. 2*F–H* for typical cell morphologies). For each injected neuron, the length of each filopodium was measured (including those that spanned multiple focal planes), and a histogram and cumulative histogram of filopodial length were calculated. These were then averaged to arrive at a mean histogram (Table 2; Fig. 6*C*) and mean cumulative histogram (Table 3; Fig. 6*D*) for each genotype.

Filopodial length distributions for wild-type and CyO/CyO embryos are very similar, with a peak at 1–2 μm, which falls off rapidly to a maximum of 7–8 and 9–10 μm, respectively (Fig. 6*C*). The histogram for *robo* mutant embryos is skewed toward longer filopodia, with a smaller peak at 1–2 μm and a more gently falling curve out to a higher maximum of 11–12 μm. The curve for heterozygous embryos is close to that for wild type but is slightly elevated in the region of 4–7 μm.

These trends are clearer in the cumulative histograms (Fig. 6*D*). Again the *robo* curve lies above the two control curves (for lengths ≥2 μm), and the heterozygous curve lies between the two. *t* tests between the various genotypes (Table 3) show that the differences between *robo* and heterozygous embryos are highly significant ($p < 0.01$) for values 2–8 μm, the differences between CyO/CyO and +/+ are not significant, and the difference between heterozygotes and +/+ is significant at 4 and 6 μm.

Mean filopodial length was 3.10 ± 0.12 μm ($n = 278$) for *robo*/*robo* embryos, 2.36 ± 0.07 μm ($n = 398$) for *robo*/CyO embryos, 2.19 ± 0.09 μm ($n = 200$) for CyO/CyO embryos, and

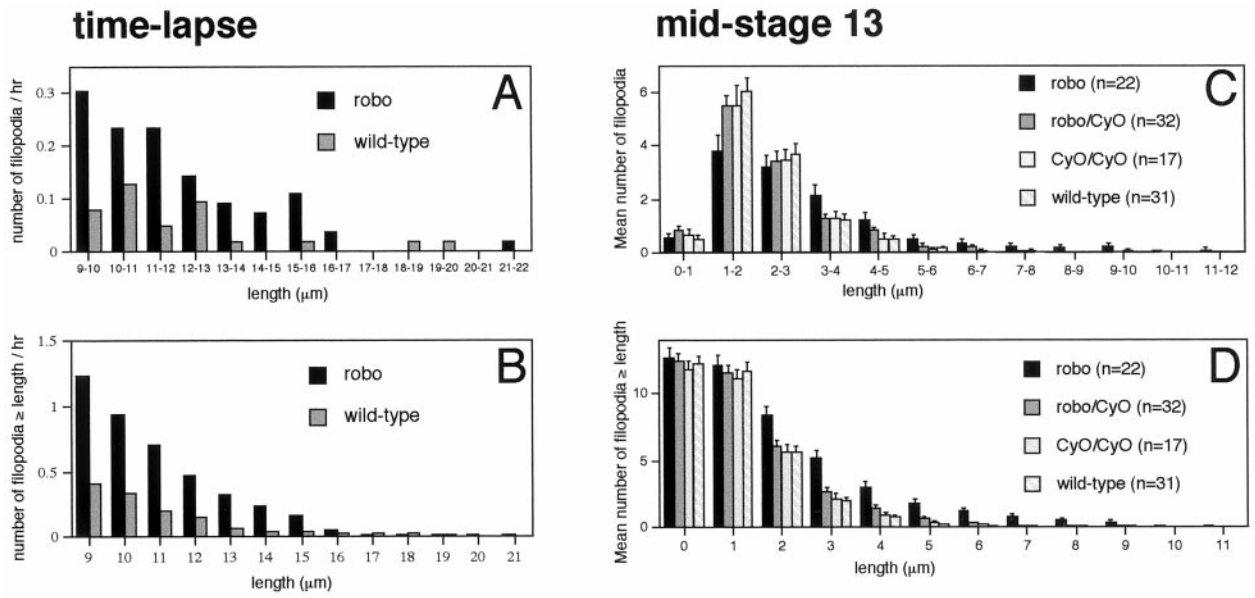

Figure 6. Filopodial length distributions for RP2 in time-lapse sequences *(A, B)* and fixed midstage 13 embryos *(C, D)*. *A*, RP2 filopodial length distributions in time-lapse sequences. Filopodia ≥9 μm were measured in wild-type ($n = 17$) and *robo* ($n = 22$) time-lapse sequences, and the results for each genotype were pooled and normalized for the total duration of sequences (55.8 hr for *robo*; 63.4 hr for wild-type) (see Materials and Methods for details), resulting in a histogram of the number of filopodia of a given length per hour. *B*, RP2 cumulative filopodial length distributions in time-lapse sequences. *Graph* shows the number of filopodia more than or equal to a given length per hour for *robo* and wild-type sequences. *C*, *D*, Filopodial length distributions in fixed midstage 13 embryos. Figure 2*F–H* shows single-plane projections of typical cells from these data sets. *n* values give total number of cells injected for each genotype. *C*, RP2 filopodial length distributions in midstage 13 embryos for four genotypes: *robo*/*robo*, *robo*/CyO, CyO/CyO, and wild-type. *D*, RP2 cumulative filopodial length distributions in midstage 13 embryos for the four genotypes. Error bars represent SEM.

Table 2. Histogram of filopodial length for RP2 in midstage 13 embryos

μm	*robo*/*robo* ($n = 22$)	*robo*/CyO ($n = 32$)	CyO/CyO ($n = 17$)	+/+ ($n = 31$)
0–1	0.55 ± 0.18	0.84 ± 0.17	0.65 ± 0.23	0.52 ± 0.13
1–2	3.82 ± 0.59	5.50 ± 0.42	5.53 ± 0.74	6.07 ± 0.50
2–3	3.22 ± 0.43	3.44 ± 0.37	3.47 ± 0.40	3.68 ± 0.39
3–4	2.18 ± 0.33	1.25 ± 0.19	1.29 ± 0.27	1.23 ± 0.24
4–5	1.22 ± 0.25	0.81 ± 0.15	0.53 ± 0.17	0.52 ± 0.12
5–6	0.50 ± 0.16	0.25 ± 0.11	0.12 ± 0.08	0.16 ± 0.07
6–7	0.36 ± 0.12	0.22 ± 0.09	0.06 ± 0.06	0.03 ± 0.03
7–8	0.23 ± 0.09	0.063 ± 0.04	0.06 ± 0.06	0.03 ± 0.03
8–9	0.18 ± 0.08	0 ± 0	0 ± 0	
9–10	0.23 ± 0.09	0.03 ± 0.03	0.06 ± 0.06	
10–11	0.05 ± 0.05	0.03 ± 0.03		
11–12	0.09 ± 0.06			

Values show mean ± SEM. Numbers in parentheses give the number of embryos injected.

2.15 ± 0.05 μm ($n = 379$) for wild-type embryos, with ranges of 0.8–11.7 μm, 0.6–10.0 μm, 0.8–9.7 μm, and 0.7–7.7 μm, respectively.

The average number of filopodia per cell (i.e., the data value for 0 μm in the cumulative histogram) was ~12 for all four genotypes. As seen in the first row of Table 3, the differences between genotypes was not significant.

Axonal trajectory and filopodial length distributions of pCC in *roundabout* embryos

To determine whether the effects of the *robo* mutation on RP2 growth cone morphology apply to other neurons, we examined the interneuron pCC in fixed embryos. Figure 7*A–C* gives examples of pCC's axonal morphology in *robo* mutant embryos and heterozygous embryos. At midstage 13, in heterozygotes, pCC's growth cone has extended ipsilaterally to the vicinity of the posterior commissure in the next anterior segment (Fig. 7*A*). In *robo* mutants, pCC's growth cone has typically crossed the midline and is extending up the contralateral longitudinal connective (Fig. 7*B*). Commonly, however, we find that pCC explores both ipsilateral and contralateral directions, bifurcating in the anterior commissure (Fig. 7*C*). Furthermore, pCC's growth cone is often highly branched near the midline (Fig. 7*B*).

Measurements of filopodial length for pCC produced results similar to those for RP2 (Tables 4, 5; Fig. 7*D*,*E*): *robo*/*robo* ($n = 14$) embryos tended to have longer filopodia than *robo*/CyO ($n = 22$) embryos, but the total number was not significantly different. In this case, however, the average number of filopodia per neuron (~24) is roughly twice that of RP2 (~12). At midstage 13, pCC's

Table 3. Cumulative histogram of filopodial length for RP2 in midstage 13 embryos

μm	*robo*/*robo* ($n = 22$)	*robo*/*robo* versus *robo*/CyO *p* value	*robo*/CyO ($n = 32$)	*robo*/CyO versus +/+ *p* value	+/+ ($n = 31$)	+/+ versus CyO/CyO *p* value	CyO/CyO ($n = 17$)
0	12.64 ± 0.84	0.85	12.44 ± 0.60	0.80	12.23 ± 0.60	0.63	11.77 ± 0.72
1	12.09 ± 0.76	0.59	11.59 ± 0.52	0.88	11.71 ± 0.58	0.51	11.12 ± 0.68
2	8.36 ± 0.65	0.005	6.09 ± 0.39	0.45	5.65 ± 0.46	0.94	5.59 ± 0.53
3	5.14 ± 0.57	0.0007	2.66 ± 0.34	0.12	1.97 ± 0.28	0.74	2.12 ± 0.35
4	3.00 ± 0.35	0.0008	1.41 ± 0.26	0.04	0.74 ± 0.17	0.78	0.82 ± 0.23
5	1.73 ± 0.30	0.003	0.59 ± 0.19	0.09	0.23 ± 0.09	0.64	0.29 ± 0.11
6	1.18 ± 0.22	0.002	0.34 ± 0.11	0.02	0.06 ± 0.04	0.30	0.18 ± 0.10
7	0.77 ± 0.19	0.003	0.13 ± 0.07	0.26	0.03 ± 0.03	0.34	0.12 ± 0.08
8	0.55 ± 0.14	0.004	0.06 ± 0.04				0.06 ± 0.06
9	0.36 ± 0.12	0.03	0.06 ± 0.04				0.06 ± 0.06
10	0.14 ± 0.07	0.21	0.03 ± 0.03				
11	0.09 ± 0.06						

Values show average number of filopodia more than or equal to given length ± SEM. *p* values give Student's *t* test comparison of genotypes in adjacent columns. Numbers in parentheses give the number of embryos injected.

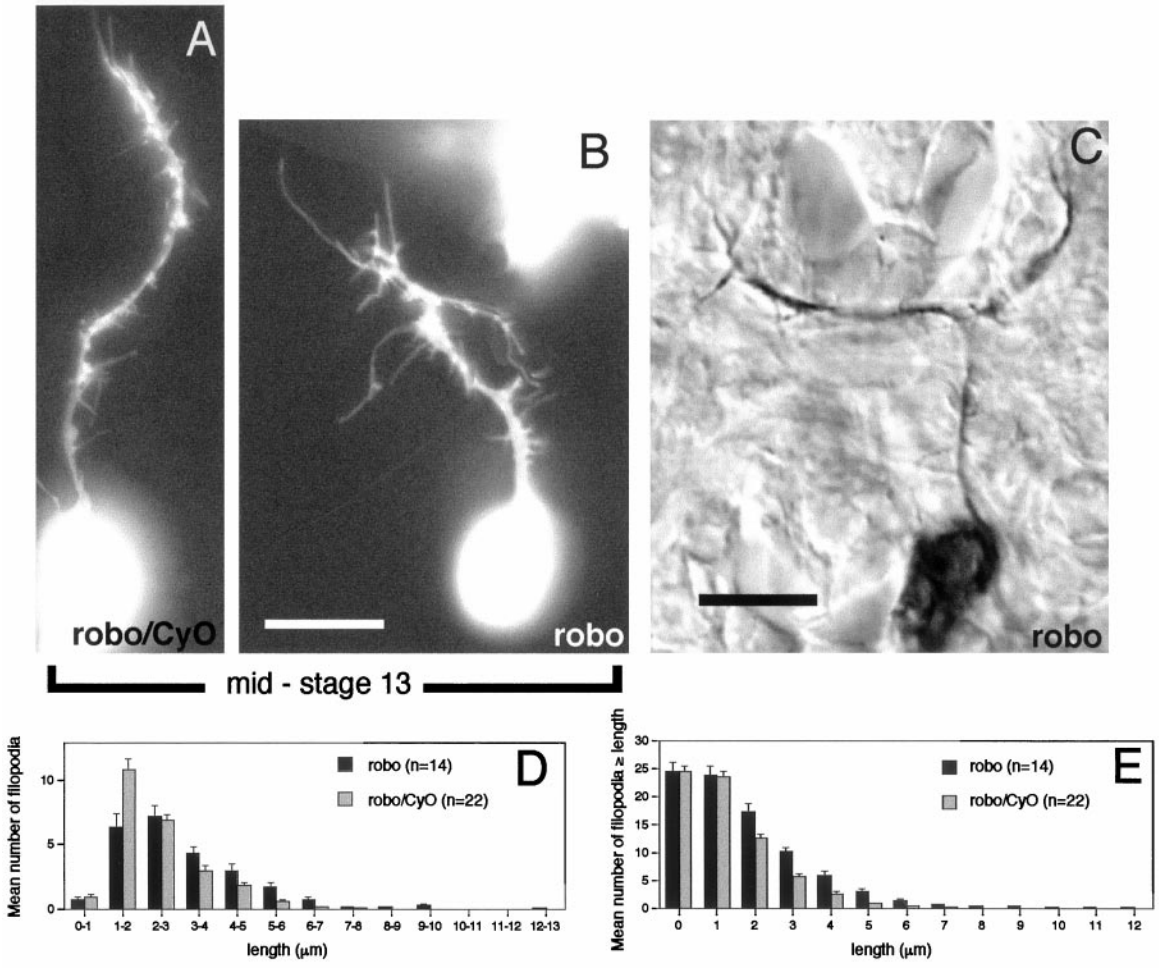

Figure 7. Growth cone morphologies and filopodial length distributions of pCC. *A*, Typical pCC growth cone at midstage 13 in *robo*/CyO embryo. pCC has a single dominant branch extending ipsilaterally along the connectives, with filopodia ranging from ~1 to 4 μm in length. *B*, pCC in midstage 13 *robo* embryo. pCC is in the process of crossing the midline and exhibits longer filopodia and a high degree of branching. *C*, pCC in stage 14 *robo* embryo. pCC has bifurcated into ipsilateral and contralateral branches. *D*, pCC filopodial length distributions in midstage 13 embryos for two genotypes: *robo*/*robo* and *robo*/CyO. *E*, pCC cumulative filopodial length distributions in midstage 13 embryos for the two genotypes. Scale bars (shown in *B* for *A* and *B*): 10 μm. Error bars represent SEM.

Table 4. Histogram of filopodial length for pCC in midstage 13 embryos

μm	*robo*/*robo* (n = 14)	*robo*/CyO (n = 22)
0–1	0.64 ± 0.20	0.91 ± 0.20
1–2	6.36 ± 1.10	10.91 ± 0.80
2–3	7.21 ± 0.82	6.96 ± 0.42
3–4	4.29 ± 0.53	2.96 ± 0.38
4–5	2.93 ± 0.52	1.77 ± 0.24
5–6	1.71 ± 0.32	0.55 ± 0.17
6–7	0.64 ± 0.20	0.18 ± 0.08
7–8	0.14 ± 0.10	0.09 ± 0.06
8–9	0.14 ± 0.10	
9–10	0.21 ± 0.11	
10–11	0.00 ± 0.00	
11–12	0.00 ± 0.00	
12–13	0.07 ± 0.07	

Values show mean ± SEM. Numbers in parentheses give the number of embryos injected.

Table 5. Cumulative histogram of filopodial length for pCC in midstage 13 embryos

μm	*robo*/*robo* (n = 14)	*robo*/CyO (n = 22)	p value
0	24.36 ± 1.82	24.32 ± 0.94	0.98
1	23.71 ± 1.76	23.41 ± 0.90	0.88
2	17.36 ± 1.27	12.50 ± 0.70	0.003
3	10.14 ± 0.76	5.55 ± 0.47	<0.0001
4	5.86 ± 0.69	2.59 ± 0.33	0.0005
5	2.93 ± 0.43	0.82 ± 0.19	0.0003
6	1.21 ± 0.26	0.27 ± 0.10	0.004
7	0.57 ± 0.14	0.09 ± 0.06	0.005
8	0.43 ± 0.14		
9	0.29 ± 0.13		
10	0.07 ± 0.07		
11	0.07 ± 0.07		
12	0.07 ± 0.07		

Values show average number of filopodia more than or equal to given length ± SEM. p values give Student's t test comparison of the two genotypes. Numbers in parentheses give the number of embryos injected.

axon is approximately twice as long as RP2's (compare Fig. 2*F* with Fig. 7*A*).

Mean filopodial length was 3.09 ± 0.09 μm (n = 341) for *robo*/*robo* embryos and 2.35 ± 0.05 μm (n = 535) for *robo*/CyO embryos, with ranges of 0.6–12.8 μm and 0.7–7.3 μm, respectively.

DISCUSSION

robo encodes an axon guidance receptor that controls midline crossing in the CNS of the *Drosophila* embryo. In this study we have attempted to understand Robo's effect on growth cone dynamics. Specifically we wished to compare the behavior of an identified ipsilaterally projecting neuron in wild-type embryos with that same cell in *robo* mutant embryos where it now crosses the midline. We first showed that as well as the interneurons previously reported the ipsilaterally projecting motorneuron RP2 can project contralaterally in *robo* mutants. In addition, we find that both RP2 and pCC can bifurcate into ipsilateral and contralateral branches and that RP2 can also be misrouted posteriorly. Time-lapse observations of RP2 show that filopodia projecting across the midline can persist for longer periods and can develop into neurites in *robo* embryos, whereas in wild-type embryos they are quickly retracted. Furthermore, *robo* mutant growth cones exhibit an excess of longer filopodia that are not restricted to pathway directions. Such filopodia often thicken, resulting in a more highly branched growth cone. Filopodial length distributions of RP2 and pCC in fixed midstage 13 embryos again showed that *robo* mutant growth cones have longer filopodia, although the total number of filopodia is unchanged. This total is different for RP2 (12) and pCC (24), suggesting that the number of filopodia may be characteristic for a particular cell at a particular stage. Alternatively, given that pCC's axon is approximately twice as long as RP2's at midstage 13, the number of filopodia may simply reflect the length of the axon. Cells from heterozygous embryos have filopodial length distributions that lie between those for wild-type and *robo* embryos. This result is compatible with previous reports that Robo function is dosage sensitive (Kidd et al., 1998b) and suggests that dosage-sensitive effects on axonal trajectories may be attributable to a graded effect on filopodial length.

The original model for Robo proposed the existence of a midline repellent ligand for which Robo was the receptor. Our results show that Robo's effects are not confined to the midline. In addition to preventing axons from crossing the midline, Robo also appears to inhibit filopodial extension and subsequent branch formation throughout the neuropile. Recently, *in vitro* binding studies (Brose et al., 1999) and genetic analysis (Kidd et al., 1999) have identified Robo's ligand as the extracellular matrix protein Slit. As expected, in the CNS *slit* is only transcribed by the midline glia. The location of the Slit protein, however, is less clear. Antibodies raised against a C-terminal fragment of the protein (Rothberg et al., 1988, 1990) show that Slit is found on the surface of axons throughout the neuropile. Recently it has emerged that Slit is proteolytically cleaved into two fragments, one of which, the C-terminal fragment, appears to be more readily diffusible (Brose et al., 1999). Thus, different antibodies may recognize different protein fragments with different expression patterns. Furthermore, evidence exists that Slit can function as a diffusible chemorepellent both *in vitro* (Brose et al., 1999) and in the *Drosophila* embryo (Kidd et al., 1999). These studies, together with our results, suggest that Slit, or a fragment thereof, may interact with Robo in regions of the neuropile away from the midline. Our results reinforce the concept that accurate growth cone guidance depends on a delicate balance of multiple attractive and repulsive cues. When a factor such as Robo is removed, the highly stereotypic trajectories of identified neurons are replaced with more variable results. Thus in the case of both RP2 and pCC, ipsilateral axons do not simply cross the midline but exhibit various trajectories and may even bifurcate into multiple axons.

One aim of this study was to gain a better understanding of the mechanism of Robo-mediated midline repulsion by observing growth cone behavior in mutant embryos. We can report three main effects on growth cones in *robo* mutants: (1) medial filopodia tend to remain extended across the midline for longer periods and can develop into branches; (2) filopodia tend to be longer; and (3) more filopodia tend to thicken, resulting in a more highly branched morphology.

How do these effects relate to each other, and what can they tell us about the mechanism of Robo repulsion? The first observation, that medial filopodia are quickly retracted in wild-type

embryos but can persist in *robo* mutants, suggests that Robo repels axons from the midline by promoting the retraction of filopodia. During the retraction of medial filopodia we do not observe any reduction in filopodial activity in adjacent regions of the neuron. This suggests a repulsive mechanism in which only those filopodia that contact the repulsive midline cues are affected. This type of repulsion may be characteristic of situations in which growth cones must navigate in close proximity to a repulsive cue without having it affect their motility. The second observation, that filopodia tend to be longer in *robo* mutants, also suggests that Robo promotes the retraction of filopodia. Although the precise determinants of maximum filopodial length are not known, they presumably involve a changing balance of factors promoting extension and retraction. Removing a factor that promotes retraction might be expected to shift the balance toward extension, resulting in longer filopodia.

How then might Robo bring about filopodial retraction, and how might this explain the tendency for filopodia to thicken into branches? A generally accepted model for the actin-based motility of peripheral structures such as filopodia is that they extend *via* actin polymerization at the distal tip and retract *via* retrograde flow of actin filaments that are depolymerized in the proximal recycling region (for review, see Welch et al., 1997). Retrograde flow is driven by the activity of myosin motors (Lin et al., 1996) and is opposed by mechanical coupling of the actin cytoskeleton to the substrate (Suter et al., 1998). The processes of polymerization and retrograde flow occur concurrently, and it is the relative balance between them that determines whether a filopodium extends, retracts, or maintains a constant length.

One possibility, therefore, is that Robo promotes retraction by reducing the coupling between the actin cytoskeleton and the substrate. This could also explain the tendency for branches to form in *robo* mutants. *In vitro* experiments using *Aplysia* neurons have shown that when coupling between the actin cytoskeleton and an external substrate is induced, the peripheral F-actin domain of the growth cone is engorged by the microtubule-rich central domain (Suter et al., 1998). A second possibility is that Robo increases myosin activity. This is perhaps less likely given the results of myosin inhibition experiments, again using *Aplysia* growth cones. Lin et al. (1996) found that although inhibition of myosins did lead to attenuation of retrograde flow and extension of the F-actin periphery, it did not lead to engorgement. A third possibility is that Robo reduces the rate of actin polymerization. Again, this could explain the tendency for branch formation. Observations of cytoskeletal changes during axon migration in the grasshopper (O'Connor et al., 1990; Sabry and Bentley, 1991; O'Connor and Bentley, 1993) and during *in vitro* growth of *Aplysia* neurons (Lin and Forscher, 1993) suggest that accumulation of F-actin at a target site can act as a signal for the subsequent invasion of a process by microtubules (Bentley and O'Connor, 1994). The idea that Robo is involved in regulating actin polymerization is supported by its amino acid sequence data. One of the three conserved intracellular motifs in Robo has been identified as a potential binding site for Enabled (Kidd et al., 1998a). Enabled (Gertler et al., 1995) is a member of the Ena/Mena/VASP family of proteins, which are thought to facilitate actin polymerization by localizing the actin-associated protein Profilin (for review, see Hu and Reichardt, 1999). This suggests a simple model in which Robo, after binding to Slit, binds to Enabled via its intracellular domain and thereby inhibits actin polymerization. Future experiments in which the cytoskeleton is directly visualized using GFP constructs could help decide between these different models of Robo-mediated filopodial retraction.

In this study we have provided new information about Robo's function by analyzing the growth cone dynamics and morphology of an individual cell. Given that Robo is expressed on all longitudinal axons (Kidd et al., 1998a), the changes observed in the behavior and morphology of RP2 could potentially be caused by indirect effects such as changes in the position of guidance cues and not the cell-autonomous activity of Robo in RP2. We think that this is unlikely in the case of the increased filopodial length and increased branching given that similar effects were also seen for pCC. To definitively test the autonomy of Robo's effects on RP2, it will be necessary to create mosaics in which RP2 has Robo function removed in a wild-type background or in which RP2 is rescued by restoring Robo function in a *robo* mutant background. Rescue experiments have been performed for other cells using the ftz_{ng}-GAL4 driver (Kidd et al., 1998a) and should now be possible for RP2 given that GAL4 drivers more specific to RP2 have been constructed (M. Fujioka and J. B. Jaynes, personal communication).

REFERENCES

Bentley D, O'Connor TP (1994) Cytoskeletal events in growth cone steering. Curr Opin Neurobiol 4:43–48.

Brose K, Bland KS, Wang KH, Arnott D, Henzel W, Goodman CS, Tessier-Lavigne M, Kidd T (1999) Slit proteins bind Robo receptors and have an evolutionarily conserved role in repulsive axon guidance. Cell 96:795–806.

Fan J, Raper JA (1995) Localized collapsing cues can steer growth cones without inducing their full collapse. Neuron 14:263–274.

Gertler FB, Comer AR, Juang J, Ahern SM, Clark MJ, Liebl EC, Hoffmann FM (1995) enabled, a dosage-sensitive suppressor of mutations in the *Drosophila* Abl tyrosine kinase, encodes an Abl substrate with SH3 domain-binding properties. Genes Dev 9:521–533.

Hu S, Reichardt LF (1999) From membrane to cytoskeleton: enabling a connection. Neuron 22:419–422.

Kapfhammer JP, Raper JA (1987) Collapse of growth cone structure on contact with specific neurites in culture. J Neurosci 7:201–212.

Kidd T, Brose K, Mitchell KJ, Fetter RD, Tessier-Lavigne M, Goodman CS, Tear G (1998a) roundabout controls axon crossing of the CNS midline and defines a novel subfamily of evolutionarily conserved guidance receptors. Cell 92:205–215.

Kidd T, Russell C, Goodman CS, Tear G (1998b) Dosage-sensitive and complementary functions of *roundabout* and *commissureless* control axon crossing of the CNS midline. Neuron 20:25–33.

Kidd T, Bland KS, Goodman CS (1999) Slit is the midline repellent for the Robo receptor in *Drosophila*. Cell 96:785–794.

Kolodziej PA, Jan LY, Jan YN (1995) Mutations that affect the length, fasciculation, or ventral orientation of specific sensory axons in the *Drosophila* embryo. Neuron 15:273–286.

Li H, Chen J, Wu W, Fagaly T, Zhou L, Yuan W, Dupuis S, Jiang Z, Nash W, Gick C, Ornitz DM, Wu JY, Rao Y (1999) Vertebrate Slit, a secreted ligand for the transmembrane protein Roundabout, is a repellent for olfactory bulb axons. Cell 96:807–818.

Lin CH, Forscher P (1993) Cytoskeletal remodeling during growth cone-target interactions. J Cell Biol 121:1369–1383.

Lin CH, Espreafico EM, Mooseker MS, Forscher P (1996) Myosin drives retrograde F-actin flow in neuronal growth cones. Neuron 16:769–782.

Murray MJ, Merritt DM, Brand AH, Whitington PM (1998) In vivo dynamics of axon guidance in the *Drosophila* embryo: a time-lapse study of an identified motorneuron. J Neurobiol 37:607–621.

O'Connor TP, Bentley D (1993) Accumulation of actin in subsets of pioneer growth cone filopodia in response to neural and epithelial guidance cues *in situ*. J Cell Biol 123:935–948.

O'Connor TP, Duerr JS, Bentley D (1990) Pioneer growth cone steering decisions mediated by single filopodial contacts *in situ*. J Neurosci 10:3935–3946.

Patel NH (1994) Imaging neuronal subsets and other cell types in whole-mount *Drosophila* embryos and larvae using antibody probes. In: Methods in cell biology (Goldstein LSB, Fyrberg EA, eds), pp 445–487. San Diego: Academic.

Rothberg JM, Hartley DA, Walther Z, Artavanis-Tsakonas S (1988) slit: an EGF-homologous locus of *D. melanogaster* involved in the development of the embryonic central nervous system. Cell 55:1047–1059.

Rothberg JM, Jacobs JR, Goodman CS, Artavanis-Tsakonas S (1990) slit: an extracellular protein necessary for development of midline glia and commissural axon pathways contains both EGF and LRR domains. Genes Dev 4:2169–2187.

Seeger M, Tear G, Ferres-Marco D, Goodman CS (1993) Mutations affecting growth cone guidance in *Drosophila*: genes necessary for guidance toward or away from the midline. Neuron 10:409–426.

Stoeckli ET, Sonderegger P, Pollerberg GE, Landmesser LT (1997) Interference with Axonin-1 and NrCAM interactions unmasks a floor-plate activity inhibitory for commissural axons. Neuron 18:209–221.

Suter DM, Errante LD, Belotserkovsky V, Forscher P (1998) The Ig superfamily cell adhesion molecule, apCAM, mediates growth cone steering by substrate-cytoskeletal coupling. J Cell Biol 141:227–240.

Welch MD, Mallavarapu A, Rosenblatt J, Mitchison TJ (1997) Actin dynamics *in vivo*. Curr Opin Cell Biol 9:54–61.

Zallen JA, Yi BA, Bargmann CI (1998) The conserved immunoglobulin superfamily member SAX-3/Robo directs multiple aspects of axon guidance in *C. elegans.* Cell 92:217–227.